Efficient structural optimisation of a 20 MW wind turbine blade

Efficient structural optimisation of a 20 MW wind turbine blade

S Scott[1], P Greaves[2], P M Weaver[1], A Pirrera[1] and T Macquart[1]

[1] Bristol Composites Institute (ACCIS), University of Bristol, BS8 1TR, UK
[2] Offshore Renewable Energy Catapult, Blyth, NE24 1LZ, UK

E-mail: ss1870@bristol.ac.uk, terence.macquart@bristol.ac.uk

Abstract. This paper presents, through the structural design of a 20 MW wind turbine blade, a selection of novel analysis and optimisation methods for wind turbines. These methods are integrated in the software—**A**eroelastic **T**urbine **O**ptimisation **M**ethods (ATOM). A key feature is the novel, computationally-efficient piecewise linear model for running rapid design load case simulations (up to 16 times speed-up over conventional methods). Further, a comprehensive set of realistic design constraints is also proposed to ensure structural feasibility and aeroelastic stability. To demonstrate these methods, a sequential gradient-based optimisation process is employed, relying on the globally convergent method of moving asymptotes (GCMMA). The process begins with an aerodynamic optimisation to generate twist distributions, followed by an iterative loop during which load envelope updates and 'frozen-load' blade structural optimisations are performed independently. Aeroelastic loads are therefore considered, but are not directly optimised for. The present study investigates the structural design of a 20 MW wind turbine blade with hybrid carbon-glass spar caps. The optimised 122 m blade is found to have a mass of 83,622 kg, which decreases to 81,396 kg (-2.66%) with the addition of sweep. The GCMMA is found to converge successfully at each structural optimisation step. By contrast, the iterative loop is observed to oscillate, albeit within small bounds. Finally, results suggest that convergence of multi-step optimisation methods for aeroelastic blade design may not be guaranteed if design variables inducing aeroelastic couplings are considered.

1. Introduction

The system level design of wind turbines is inherently a coupled problem with many complex design trade-offs. As a result, integrating as many facets of the problem as possible into a single holistic design process can lead to more economically viable turbine designs than designing components iteratively and in isolation. The integrated design of wind turbine (WT) systems is possible with multi-disciplinary optimisation (MDO) techniques, as the complex design trade-offs can be navigated algorithmically. In addition to providing better solutions than non-integrated methods, MDO allows the designer to investigate and compare turbine designs at the conceptual level, e.g. number of blades/rotors, up/downwind rotor [1], aeroelastic tailoring [2].

The economic viability of a turbine design can be measured by the levelised cost of energy (LCoE). When estimating LCoE at the system level, it is not realistic to consider every facet of the WT lifecycle in extreme detail for two reasons: some input data—e.g. site conditions and material costs—are uncertain by nature; and other data may be too computationally demanding to acquire e.g. detailed stress fields/wake effects. Thus, a balance must be struck between maximising confidence in LCoE estimations, whilst minimising computational costs. Given a

limited amount of computational resource, it is logical to focus design detail on the most LCoE-driving components. Arguably, the rotor has the greatest influence on LCoE, as annual energy production (AEP) is predominantly driven by the aeroelastic properties of the blade, and, whilst rotors typically account for a relatively small part of the direct cost, the indirect influence of aerodynamic and inertial loading on the sizing of drivetrain, tower and foundations is significant. Thus, WT rotor design is often a focus area for WT MDO studies.

There are many examples in the literature addressing the combined issue of WT MDO whilst minimising computational effort; all of them placing specific emphasis on the rotor design. For example, the Horizontal Axis Wind Turbine Optimisation Tool (`HAWTOpt2`) developed at Denmark Technical University (DTU) utilises a linearised model for fast fatigue load estimation in the frequency domain [3], in addition to a method for estimating extreme loads with reduced simulation time [4]. These tools have been used in MDO studies to optimise aeroelastic tailored blade designs [2, 5], whereby objective functions of a comparative nature have been used, such as $\mathrm{AEP}/\mathrm{AEP}_{\mathrm{baseline}}$. However, the use of non-physically driven constraints (e.g. loads not exceeding those of the baseline) may pose unrealistic limits on the design space.

Researchers at Politecnico di Milano and the Technical University of Munich have developed the Code for Performance Maximization (`Cp-Max`), in which a multi-level approach is taken to achieve aero-stuctural optimisation of rotor and tower [6, 7]. The multi-level framework ensures that each optimisation problem is well-posed and likely to converge. The two independent sub-problems (maximise AEP, and minimise initial capital cost) are aero-structurally linked by outer optimisation macro variables—such as solidity and taper—enforced as equality constraints on the sub-levels, aiding the outer optimisation to find LCoE-optimal solutions. A drawback of the multi-level approach is that some important aeroelastic effects are not considered by the optimiser, which may lead to sub-optimal solutions. For example, the effect of blade flapwise stiffness (driven largely by spar cap thickness) on swept area, and hence AEP, is not captured by the optimiser; this effect being more significant for longer blades. Similarly, the effect of torsional stiffness on twist angles and AEP, critically important for the aeroelastic tailoring of blades, cannot be optimised.

Whilst the authors have pointed out some shortfalls of current LCoE-optimisation practices in the literature—e.g. missing aeroelastic design couplings, providing non-physically driven bounds on the design—this paper does not aim to address the full LCoE-aero-structural design problem directly, this being the subject of future publications. Instead, the present paper aims to demonstrate the efficacy of a novel set of design and optimisation methods which are highly suitable for addressing the full problem. Efficacy of the methods is demonstrated by a case study of slightly reduced scope: the structural design of a 20 MW turbine blade with hybrid carbon-glass spar caps, with and without rearward sweep. The novel design methods employed here are part of the holistic MDO software for WTs named **A**eroelastic **T**urbine **O**ptimisation **M**ethods (`ATOM`) [8, 9], and are listed as follows:

- A piece-wise linear turbine model for rapid design load case (DLC) simulations as per IEC/DNV standards [10, 11]. The speed-up offered by this method readily enables the re-evaluation of load envelopes during optimisation (although not done here), thus, capturing all design couplings. Further, smooth gradients are ensured even with turbulent wind fields.
- A comprehensive and solely physically driven suite of feasibility constraints are employed to ensure a realistic design space. These are also fast to compute. A key feature of the present study is the constraint on aeroelastic stability, provided by the linearised models, as this avoids the problem of structural optimisation producing unstable designs.
- The application of the globally convergent method of moving asymptotes (GCMMA) algorithm [12] to wind turbine structural optimisation. This algorithm displays efficient convergence and has some ability to avoid local minima.

The design case study presented here employs an iterative 'frozen-loads' procedure, similar to that performed with the `Cp-Max` tool ([1, 6]), whereby: (i) twist angles are optimised for maximum AEP in an independent process, (ii) load envelopes are computed from DLCs, (iii) the structure is then optimised independently. Steps (ii) and (iii) are repeated until convergence of either the loads or design variables (DVs). This approach accounts for aeroelastic effects of the changing design with each load update, however, the optimiser cannot design for aeroelastic effects.

2. Design problem

2.1. Turbine description

The model used in this work is based on the INNWIND/PoliMI 20 MW reference wind turbine (RWT) [13, 14]. However, changes of note include a monotonic prebend curvature (with upwind tip offset of 4 m), the inclusion of carbon in the spar caps, and a reduction of tilt angle. Blade length, hub height, cone angle, chord and relative thickness remain unchanged, whilst blade twist angles are optimised, parameterised using B-splines and four DVs. It is noted that prebend and sweep curvature are applied as orthogonal offsets to the beam axis and the longitudinal co-ordinate is modified so as to preserve the blade arc length, not the blade radius. Thus the effects of prebend and sweep can be considered independently from those of blade length.

A similar blade structural configuration to the RWT is employed here, with monolithic laminates in the root region, spar caps and leading/trailing edge (LE/TE) reinforcements. Further outboard, sandwich panels span the aerodynamic surfaces between spar cap and LE/TE reinforcements. The model comprises three webs. Web 1 and 2 in a spar box formation, and a third being placed on the TE panel as a panel breaker.

Material layers, their locations in the blade, and the associated DVs are described in Table 1. Gelcoat and excess resin are accounted for as non-structural masses, whilst uni-directional (UD),

Table 1. Description of blade structural and aerodynamic design variables (DVs). Some structural layers are included but are not DVs (#DVs = 0).

Layer/DV name	Blade loc.	# DVs	Comments
Shell			
Gelcoat	All over	0	0.5 mm layer, negligible stiffness, realistic mass
Biax	All over	9	Glass biax covering the whole blade (inner & outer)
Root UD	All over	5	Glass UD near the root (inner & outer)
UD glass	Spar cap	8	Glass UD in the spar cap
UD carbon	Spar cap	16	Carbon UD in the spar cap, independent SS & PS
Biax glass	Spar cap	0	Glass biax in the spar cap for buckling resistance
LE reinf.	LE	6	Glass UD in the LE
TE reinf.	TE	6	Glass UD in the TE
Balsa core	Panels	24	Balsa core, independent DVs in each blade quadrant
Excess resin	All over	0	Excess resin - non-structural mass (inner surface)
Webs			
Biax	All webs	0	6 layers of biax as sandwich skin
Balsa core	All webs	18	Balsa core, independent for each web
Internal geom.			
Spar cap start/end	Spar cap	8	Chordwise interface between spar cap & panels
TE web loc.	TE web	8	Chordwise attachment loc. of TE web
Aero. DVs			
Twist angles	NA	4	Third-order B-spline. Root is fixed.
Total structural		**108**	
Total aerodynamic		**4**	

biaxial and balsa layers are used in the skins, spar caps and webs. The hybrid spar cap is made of both UD carbon and glass. Moreover, the UD carbon can vary independently on the blades pressure and suction sides (PS & SS), allowing the optimiser to navigate the inherent performance-cost trade-off. Glass biax makes up the inner and outer layers of the shell laminate, providing a skin for the sandwich panels, and contributing significantly to the blade torsional stiffness. End-grain balsa is used as a sandwich core and provides buckling resistance in the LE/TE panels and the webs. The spar cap geometry is defined by DVs at the blade root and tip, thus the caps can either be tapered or of a constant width. Thickness DVs have the lower bound of a single layer thickness, and upper bound scaled on the aerofoil section thickness. Twist angles are bounded between $\pm 30°$.

2.2. Generation of load envelopes

In order to assess AEP and structural feasibility, it is necessary to run DLC simulations as specified by design standards [10, 11]. `ATOM` is capable of performing aero-servo-elastic simulations, in addition to the relevant pre- and post-processing of cross-sectional properties/strains. For aeroelastic simulations, `ATOM` employs blade-element-momentum (BEM) theory with a dynamic stall model for computing aerodynamic loads. A number of beam finite element solvers are available for structural dynamics (modal, linear [15] and non-linear [16]). In addition to BEM, `ATOM` can generate linear models of the WT aerodynamic states at a number of equilibrium points, which are then used in a piecewise interpolation scheme to perform rapid aero-servo-elastic simulations with turbulent wind fields. The piecewise linear simulations offer a significant speed-up over the conventional BEM method of running simulations. For example, on a desktop PC, run times for averaged 600 s simulation are compared in Table 2, where a feature of note is that the linearised model allows for greater time steps due to the unconditionally stable implicit time-marching scheme. The linearised models are ideal for power production simulations, however, the current implementation is not yet set up for idling or fault scenarios—which are instead simulated using the BEM model. In order to save on computation time without significantly compromising the relevancy of the optimised blade designs, this work employs a reduced set of DLCs, comprising DLC 1.1, 1.2, 1.3, 2.3 and 6.1 with one seed each.

Table 2. Approximate run times and speed-up averaged from 36 DLC 1.1 600 s simulations. Run on a desktop PC (quad core i7 3.40GHz).

Method	Timestep (s)	Real time (s)	speed-up
BEM	0.02	490	-
Linearised	0.02	110	4.5×
Linearised	0.1	30	16×

Load envelopes are post processed from time-histories as per DNV standards, with relevant safety factors. Ultimate loads are computed in 12 load directions (30° combinations of flapwise and edgewise) at each cross section. By rotating around 360° in the flap-edge plane both minimum and maximum cases are captured. However, the extrema torsional/axial loads must also be included. For each instance of ultimate loading found, the six load components from that time instance are saved and any repeated loads are removed. Fatigue loads are saved as full time histories from DLC 1.2. Further, full blade load sets at time instances of max deflection are also saved, for when the rotor is 10% either side of the tower azimuthal position.

2.3. Design constraints

In this work, the focus is on providing a comprehensive set of physically-driven constraints, to place realistic bounds on the design, whilst minimising computational effort. The constraints used in this work are summarised in Table 3, and described in more detail in the following.

Table 3. Summary of constraints.

Constraint	Value	Comment
Tower clearance	$> 30\%$ unloaded	Avoids tower impact [11]
Ultimate strength	< 1.0	Puck criterion
Buckling	< 1.0	Analytical panel buckling [17]
Fatigue damage	< 1.0	Linear goodman damage summation [11]
Aeroelastic stability	$\text{real}(\text{eig}(A)) < 0.0$	Real part of lin. model eigenvalues is negative
Frequency margins	$> 10\%$	1st flap/3P, 1st edge/3P, 1st flap/1st edge
Ply/core taper	$< X$ mm/m	$X_{ply} = 5$, $X_{core} = 200$
Max. laminate thickness	< 100 mm	For manufacturability

2.3.1. Tower clearance As per [11], collision between blade and tower must be avoided and "the clearance shall not be less than 30% for the rotor turning, in relation to the clearance in the unloaded state" [11]. Clearance in the unloaded state considers prebend, cone, tilt and the tower diameter at blade tip height.

2.3.2. Structural failure modes Short term strength, fatigue strength and buckling constraints are assessed within `ATOM`. Cross-sectional strains are computed from the load envelope and then input to the constraint functions. It is noted that only in-plane strains are available, therefore, features such as the trailing edge bond line are not assessed for failure. All of the failure constraints are aggregated [18], which aids convergence when many constraints are active at optimum.

Short term strength is assessed for fibre failure (FF) and inter-fibre failure (IFF) using the Puck criterion at every cross-sectional element and every cross-section. Fatigue damage is assessed using the linear Goodman analysis, described in [11], using only the longitudinal strain component and full strain-time histories in a reduced set of cross-sections/elements, due to the computational cost. Panel buckling is assessed using the Energy Research Centre of the Netherlands' (ECN) analytical model [17]. Panels are assumed to be simply supported and infinitely long at each cross-section, both conservative assumptions. A less conservative choice of reduction factor γ_{m4} is therefore used to avoid over-conservative buckling constraints. Material reduction factors for each failure mode are displayed in Table 4.

Table 4. Material reduction factors as per [11].

Reduction factor	FF	IFF	Fatigue	Buckling	
γ_{m0}	1.2	1.2	1.2	1.2	Base factor
γ_{mc}	1.08	1.0	1.08	1.08	Failure mode
γ_{m1}	1.2	1.1	1.1	1.05	Long term degradation
γ_{m2}	1.1	1.0	1.0	1.05	Temperature effects
γ_{m3}	1.3	1.0	1.3	1.1	Manufacturing effects
γ_{m4}	1.0	1.15	1.25	1.25	Accuracy of analysis
γ_{m5}	1.0	1.0	1.0	1.0	Load assumptions
Total	**2.22**	**1.52**	**2.32**	**1.96**	

2.3.3. Dynamic feasibility Aeroelastic stability is constrained using the same linearised model as for performing DLC simulations. A number of state-space models are generated, thus, if the real part of the eigenvalues of any linearised model are positive then the equilibrium state rotor/tower model is aeroelastically unstable. Consequently, the aggregated eigenvalues are constrained to be less than zero. In addition, frequency margins are applied to avoid resonant

interactions between blade/tower frequencies and the rotor 3P frequency at rated, in addition to separation between the first blade flapwise and edgewise frequencies.

2.3.4. Design for manufacture considerations Spanwise ply taper rates represent the need for a minimum spacing between ply drops, these being limited to a maximum of 5 mm change in laminate thickness per meter [19]. Core taper is also constrained in the spanwise and chordwise directions as per recommendations in [11]. Lastly, a constraint on the maximum laminate thickness is used to avoid excessively thick laminates that may be difficult to infuse consistently, without large exotherms, or for which sourcing balsa of the required thickness may be difficult. This limit is highly dependent on the chosen manufacturing process, however, a representative value of 100 mm has been chosen for this study.

3. Optimisation approach

The design studies presented here integrate both aerodynamic and structural optimisations within a nested architecture, as illustrated in Figure 1. Design detail is primarily focused in the structural optimisation, as the aerodynamic optimisation designs only the blade twist distributions with all other planform variables fixed (see Table 1 for DVs). The aerodynamic optimisation is run once at the beginning of the process and the objective is to maximise steady AEP, to ensure better comparability between the non-swept and swept blades. The structural loop then aims to find a mass-optimal internal structure for the prescribed planform.

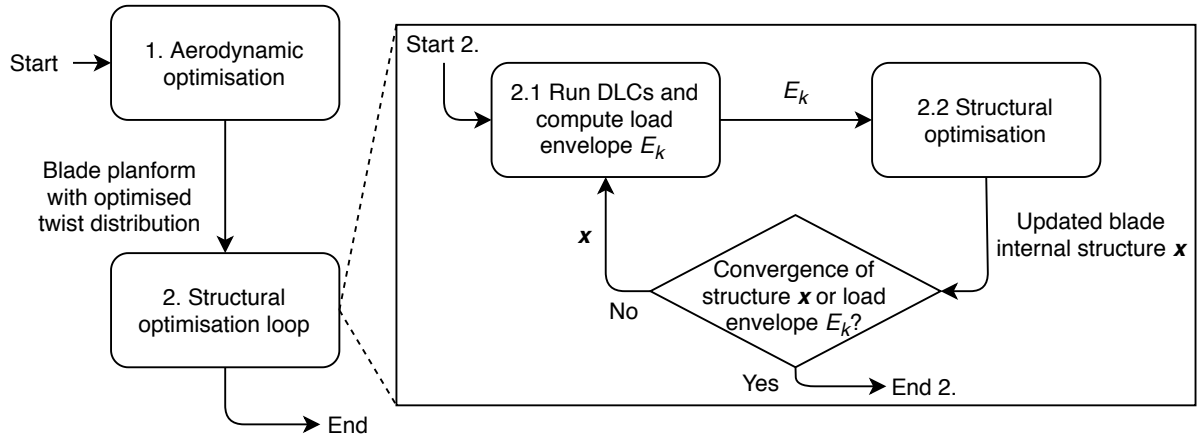

Figure 1. Diagram of the optimisation architecture.

The structural loop is an iterative procedure whereby the DLC simulations are run and load envelopes are computed, then a structural optimisation is performed with fixed, or 'frozen' loads. The loop is repeated until convergence of either the load envelopes or the structural DVs. Aeroelastic effects of changing the blade design are accounted for by updating the load envelopes, however, convergence of the loop is only possible if these effects are small. Load envelopes are primarily composed of aerodynamic and inertial/gravitational loads, thus, one possible assumption is that laminate thickness DVs have a negligible impact on aerodynamic loads and a monotonic effect on the inertial loads—which are relatively small anyway [6]. However, where this assumption would fall down is if the DVs had aeroelastic influence on the loads. An extreme example of this would be if the DVs induced an aeroelastic instability which, without the constraint on stability used here, can occur for this blade if there is not enough torsional stiffness (provided by the triax in the skins). However, ignoring extreme examples, the assumption of DVs having small effect on the aerodynamic loads is still questionable for some

of the DVs employed in this study. For example, allowing independent variation of spar cap thickness, width and position, can strongly affect the blade coupled stiffness terms which, in turn, have aeroelastic influence.

Each optimisation is a single objective minimisation, subject to non-linear inequality constraints, of the form

$$\begin{aligned} &\underset{\mathbf{x}}{\text{Minimize}} \quad f(\mathbf{x}) \\ &\text{Subject to} \quad g_i(\mathbf{x}, E_k) \leq 0; \quad i = 1, ..., m; \quad k = 1, ...n; \end{aligned} \tag{1}$$

where $\mathbf{x}$ is the vector of design variables, and g_i is the i^{th} non-linear constraint function computed using the k^{th} evalutation of the load envelope E_k. The objective function f can either take the form of f_{aero} or f_{struct}, where these are the aerodynamic objective function and an augmented mass-objective function defined respectively as:

$$f_{\text{aero}} = AEP_{\text{Baseline}}/AEP, \tag{2}$$

$$f_{\text{struct}} = M_{\text{blade}} + (\alpha - 1) \times M_{\text{CFRP}}, \tag{3}$$

where M_{blade} is the total blade mass, M_{CFRP} is the mass of carbon fibre in the blade, and α is a weighting factor for the added cost of carbon fibre—the latter taking a value of 4 as recommended by an industrial partner. It is noted that α is subject to change due to various socio-economic factors such as the price of oil, however, for research purposes this serves to illustrate the effect of the cost difference.

The algorithm used for both the aerodynamic and structural optimisations is GCMMA [12]. GCMMA is a gradient-based method that, at each iteration, generates and solves a convex subproblem that approximates the original objective and constraint functions. If the subproblem is found to be inaccurate, then the approximating functions are sequentially modified until they are conservative and an improved solution is found. Conversely to methods such as sequential qudaratic programming, GCMMA introduces curvature in the approximating constraint functions, as well as the objective, this being more appropriate for many of the constraints used in structural optimisation. GCMMA has the ability to avoid local minima and, from the authors' experience, can converge efficiently even when started from infeasible points. These two features of GCMMA make it ideal as a design tool where no 'good' baseline design is already available e.g. in the case here of moving from the INNWIND RWT all-glass design to hybrid glass-carbon spar caps.

In the present study, central finite-differences are employed with gradient evaluations parallelised across multiple CPUs. Following the final optimisation, continuous thicknesses in each cross-section are post-processed into discrete numbers of plies, in which the continuous thickness is divided by the number of plies and if the number of plies is 10% greater than a whole number it is rounded up, otherwise it is rounded down. It is noted that the all of the analysis and optimisation software used in this work is implemented in `MATLAB`.

4. Results and discussion

4.1. Convergence

The optimisation history for the non-swept blade is displayed in Figure 2, in which objectives are normalised with respect to the final value. For each individual structural optimisation, successful convergence is indicated by the asymptotic behaviour of the objective and constraint functions. Further, convergence is supported by the large number of constraints active at the optimal points. Figure 3 shows the constraint values for the final optimised baseline and is representative of the number of active constraints found in general.

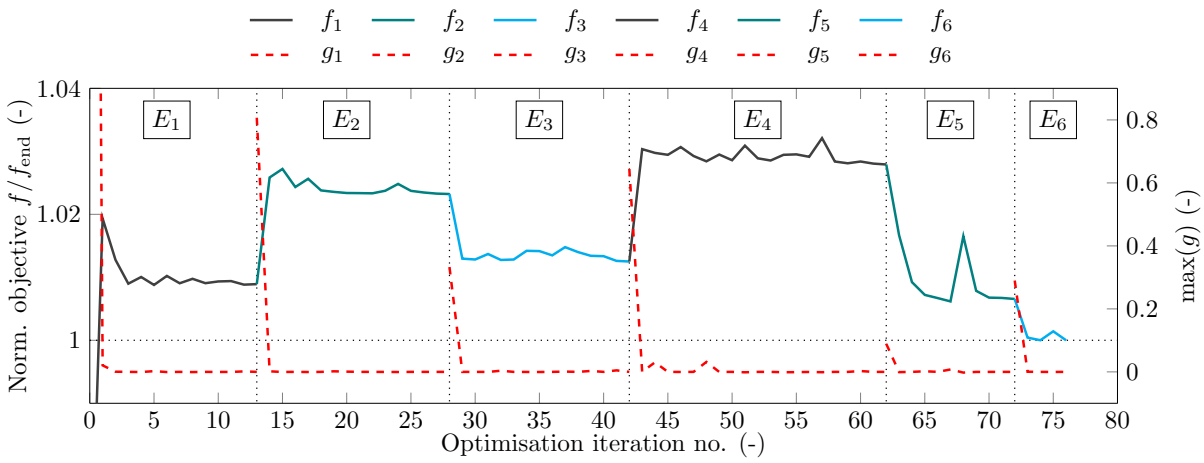

Figure 2. Optimisation history of normalised objective $f(x)/f(x_{\text{final}})$ and max. constraint function $g(x, E_k)$ at any one opti. iteration, where k refers to the k^{th} iteration of load envelope E_k. Vertical lines indicate points at which one optimisation converges and loads are updated.

As can be seen from Figure 2, some constraints are violated at each update of the load envelope E_k. In addition, the optimal objective value from each optimisation tends to oscillate without obvious convergence, albeit the oscillations are within relatively small bounds. However, the behaviour of the iterative loop cannot be said to be converging "in only a few iterations", contrary to results reported in other work [17]. This oscillatory behaviour is also displayed by the DVs and load envelopes. One possible explanation for poor convergence of the iterative loop is that the DVs influence on the load envelope, through aeroelastic couplings, is not negligible. As mentioned, spar cap asymmetry and LE/TE asymmetry, which are both featured in the current parameterisation, can affect flap-twist, edge-twist, and flap-edge coupling terms in the cross-sectional stiffness matrices. Thus, aerodynamic loads are likely reasonably sensitive to the DVs used here.

Figure 2 displays the ability of the GCMMA algorithm to converge when started from infeasible points, as is the case for all load updates, and usually only a few iterations are

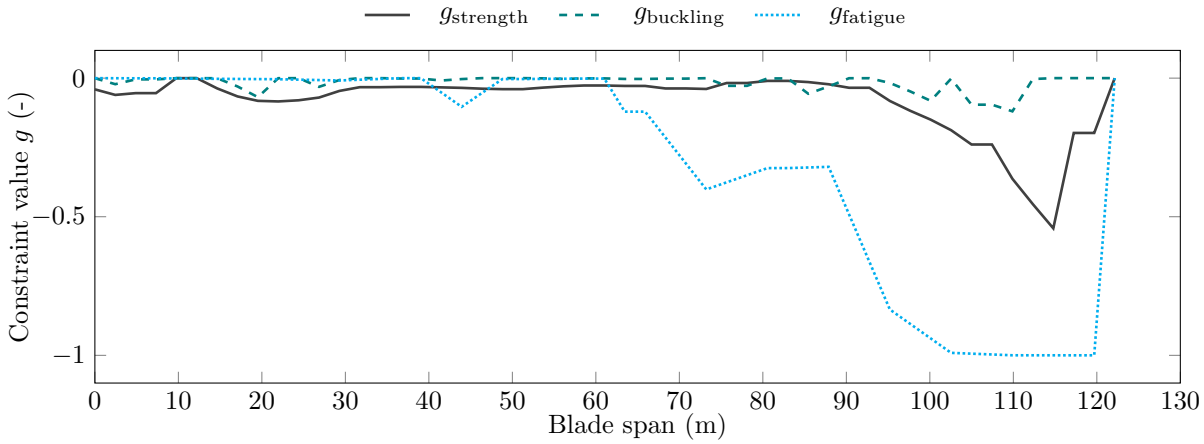

Figure 3. Spanwise variation in maximum failure constraints $g(x)$ for strength, buckling and fatigue. Results are displayed for the final non-swept blade.

required to satisfy the constraints. Another benefit of GCMMA that has been observed by the authors is the ability to avoid local minima which other algorithms would otherwise get stuck in. For example, in test cases not displayed here, GCMMA outperforms `Matlab`'s `fmincon` (with sequential quadratic programming) particularly because GCMMA would find solutions with more significant changes in spar cap width/location. A drawback of the optimisation process is the use of finite difference gradients. The accuracy of the final optimised solution is limited by the inherent error in the finite difference approximations, however, it is unlikely that a higher solution accuracy would result in any observable effects in the post-processed design.

4.2. Non-swept baseline

Important metrics for the optimised non-swept blade are displayed in Table 5, in addition to those for the PoliMI INNWIND RWT [14]. It must be noted that the INNWIND RWT is structurally infeasible within `ATOM` due to violated tower clearance, buckling and fatigue constraints. It is thought this may be due to the coarse wind field granularity used to design this turbine (10 *vs* 48 grid points used here), or potentially the omission of tower diameter in the tower clearance constraint.

The optimised non-swept blade mass is 83,622 kg. However, the blade mass objective f_{struct} is higher due to the extra weighting α for UD carbon in the spar caps. Many constraints are active at optimum, indicating a converged design. Strength, buckling and fatigue failure constraints are displayed in Figure 3. In addition, tower clearance, and maximum laminate thicknesses around the max-chord region are also active.

Strength failure constraints are primarily active in the SS spar cap, and specifically only in the UD carbon layer due to longitudinal compressive failure. The compressive strength of the

Table 5. Output metric comparisons for the optimised blade design with post-processed thicknesses. The PoliMI INNWIND RWT [14] is included for reference, however, is structurally infeasible within `ATOM`. Percentage differences compare the non-swept and swept blades.

	INNWIND RWT	Non-swept	Swept	% diff.
Blade mass objective (kg)	112784	128404	123588	-3.75
Total blade mass (kg)	112784	83622	81396	-2.66
Mass carbon UD (kg)	0	14927	14064	-5.79
Mass balsa (kg)	8633	7712	7970	3.35
Mass glass UD (kg)	56192	22199	22017	-0.82
Mass glass BIAX (kg)	4652	30230	28793	-4.75
Mass glass TRIAX (kg)	34787	0	0	0
LCoE (INNWIND cost model [13]) (€/MWh)	94.19	94.65	94.62	-0.04
AEP (GWh)	94.96	95.38	95.20	-0.19
$Cp_{\max}$ (-)	0.45	0.46	0.46	-0.35
Rotor swept area @ rated (m^2)	50449	50375	50504	0.26
Max. Flapwise tip displacement (m)	22.549	16.058	15.997	-0.38
Max. Torsional root moment (Nm)	2.86×10^6	2.41×10^6	2.57×10^6	6.47
Max. Edgewise root moment (Nm)	1.29×10^8	1.12×10^8	1.04×10^8	-7.83
Max. Flapwise root moment (Nm)	2.18×10^8	2.03×10^8	1.91×10^8	-5.52
Max. Hub-centre torque moment (Nm)	1.71×10^8	1.34×10^8	1.27×10^8	-4.61
Max. Tower-top thrust force (N)	7.00×10^6	6.77×10^6	6.23×10^6	-7.98
DEL: Torsional root moment (Nm)	1.45×10^6	1.51×10^6	1.32×10^6	-12.55
DEL: Edgewise root moment (Nm)	1.60×10^8	1.22×10^8	1.15×10^8	-5.77
DEL: Flapwise root moment (Nm)	1.15×10^8	1.02×10^8	9.14×10^7	-9.97
DEL: Hub centre-torque moment (Nm)	1.16×10^8	8.95×10^7	8.46×10^7	-5.39
DEL: Tower top-thrust force (N)	3.10×10^6	2.68×10^6	2.55×10^6	-5.02

UD carbon is around half of its tensile strength, and the load envelope is considerably more dominant in the positive flapwise direction (acting to load the SS in compression), therefore, compression failure in the SS is a primary design driver. Buckling failure is design driving along the whole length of the blade and mainly in the sandwich panels, however, the inboard section of the SS spar cap also has some active buckling constraints. Buckling predominantly drives the balsa core thicknesses and is most significant in the TE SS panel around max-chord to mid-span, due to the combination of load envelopes being more severe in the positive flapwise direction and the lack of curvature in this panel. Fatigue failure is design driving mostly from root to mid-span and most critical in the TE reinforcement (glass BIAX layer) and SS spar cap (UD carbon layer). The maximum laminate thickness constraints are primarily active in the SS TE panel and the SS spar cap—around the max chord to mid-span region. The effect of this constraint being active is to force the optimiser to utilise spar cap width, instead of spar cap thickness (or web location rather than balsa thickness) to satisfy the strength and buckling constraints.

Spar cap carbon and glass layer thicknesses are displayed by the dashed lines in Figure 4. Given the performance-cost trade off, the optimiser chooses to utilise UD glass mainly in the root and tip regions, whereas the mid-span utilises predominantly UD carbon. Evidently, the extra stiffness provided by UD carbon is worth the added cost in this region of the blade, which is mostly driven by the tower clearance and strength constraints. Less carbon is required in the root region due to the cantilever constraint which inhibits bending rotations at this point, in addition to the increased second moment of area and thick root reinforcement layers contributing to bending stiffness. Near the tip, the blade loads drop off and thus a higher percentage of glass is deemed cost-efficient for providing bending stiffness. The difference in carbon thickness between SS and PS can be attributed to the aforementioned load envelope asymmetry and disparity between compressive and tensile strength of UD carbon.

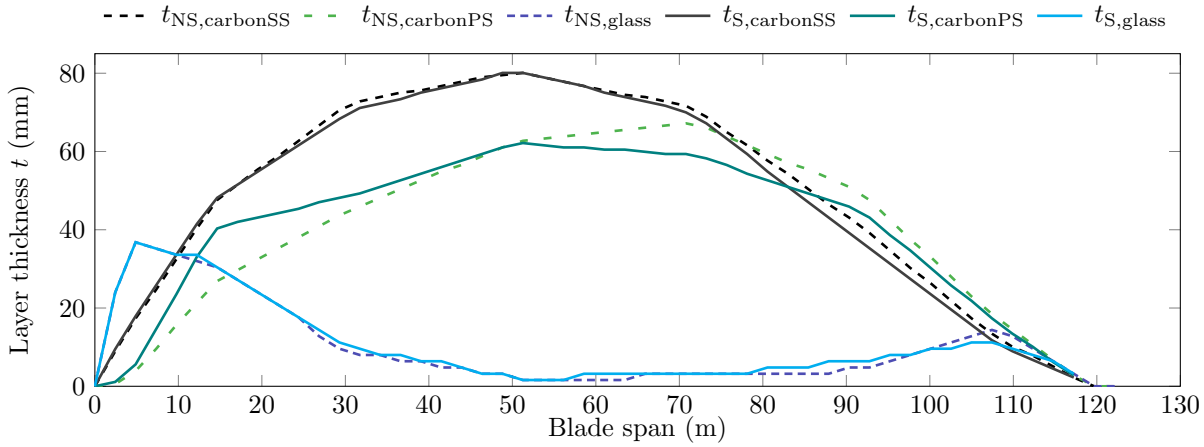

Figure 4. Comparison of layer thicknesses in the spar caps. Dashed lines, or 'NS', indicate the non-swept blade and solid lines, or 'S', the swept blade.

4.3. Swept design

Metrics for the optimised swept blade, and percentage differences w.r.t. the non-swept blade are displayed in Table 5. It can be seen that a 3.75% reduction in mass objective is found, where this is driven mainly by the reduction in UD carbon (see Figure 4). The reduction in mass for the swept blade can be attributed to the passive load alleviation effect of adding blade sweep, as the blade length does not increase. Load alleviation can be observed in nearly all of the ultimate

and fatigue load components displayed in Table 5, where sweep has effect on the flapwise/thrust loads and the reduced blade mass affects the edgewise loads. However, the drawback of sweep is that the AEP is marginally reduced. These results confirm those found in other work, however, a contrasting feature is the relatively small increase in blade root torsional loads with sweep, and the reduction of torsional DEL as opposed to the increase found in [2]. Interestingly, whilst the maximum nose-down torsional load increases with sweep (6.5%), the nose-up loads decrease quite significantly (-34% in ULT). DELs only consider load cycle amplitude, not mean, therefore, a decrease is found.

Active failure constraints display similar trends to those discussed for the non-swept blade. However, more compressive strength constraints are active in the PS spar cap near the root. This is accompanied by a shifting of UD carbon thickness further inboard in the PS spar cap, and reduction of the SS spar cap carbon thickness in the outboard section, as seen in Figure 4. In addition, the aeroelastic stability constraint becomes active for some of the load iterations, though not all. If this constraint was not employed, the structurally optimal blade may have been unstable and produced a significant increase in the subsequent load envelope update.

5. Conclusions

This work demonstrates the ability of the WT MDO tool, `ATOM`, to perform structural design of a 122 m blade employing hybrid carbon/glass spar caps, with and without sweep curvature. Key to `ATOM`'s implementation is striking a balance between providing sufficient design detail suitable for a system LCoE estimate whilst minimising computational cost. Therefore, the optimisation is subject to a comprehensive set of realistic, yet computationally efficient, design constraints including: strength, fatigue, tower clearance, buckling, aeroelastic stability, and design for manufacture. In addition, load envelopes are generated using rapid simulations run with a novel piecewise linear model of the turbine, which, in addition, demonstrates the ability to capture load alleviation effects due to sweep. The optimal non-swept blade has mass 83,622 kg and the swept blade has mass 81,396 kg (-2.66%), the reduction reflective of the load alleviation. Note that the implementation of sweep here preserves blade arc length, and not radius. Both designs are predominantly driven by compressive strength of the UD carbon in the SS spar cap, buckling in the sandwich panels, tower clearance, and fatigue in the TE reinforcement and SS spar cap. UD glass is favoured closer to the root and tip, whereas UD carbon is favoured in the mid-span of the spar caps. No physical limits on the structural feasibility of 20 MW turbines are highlighted by this study, although conventional layup techniques and web/mould alignment may become problematic at this scale (max chord = 8 m).

The optimisation process begins with an aerodynamic optimisation to design blade twist distributions for maximum AEP, then an iterative structural optimisation loop is performed in which load envelopes are updated, the blade internal structure is optimised, and this loop is repeated until convergence of the load envelope or DVs. The gradient-based algorithm, GCMMA, is employed and displays successful convergence, even when started from infeasible points. In contrast, the iterative loop displays oscillatory behaviour, albeit within small bounds, and is thought to be due to the aeroelastic influence of the DVs. Convergence to a high accuracy has not been observed with GCMMA, which would likely be improved by more accurate gradient information e.g. analytic or complex gradients.

Work is currently underway in applying `ATOM` to the integrated aero-structural optimisation of wind turbines. Future work aims to address the following:

- Capturing all important design couplings relevant for large wind turbine blades e.g. the swept area/AEP vs flapwise stiffness/prebend/tower clearance trade-off.
- Exploring the LCoE benefits available by opening up the aeroelastic tailored design space.

Acknowledgments
This project is funded by the Wind Blades Research Hub (WBRH), a joint collaboration between the University of Bristol and ORE Catapult.

References
[1] P. Bortolotti, A. Kapila, and C. L. Bottasso, "Comparison between upwind and downwind designs of a 10 MW wind turbine rotor," *Wind Energy Science*, vol. 4, no. 1, pp. 115–125, 2019.
[2] C. Pavese, C. Tibaldi, F. Zahle, and T. Kim, "Aeroelastic multidisciplinary design optimization of a swept wind turbine blade," *Wind Energy*, pp. 1–13, 2017.
[3] C. Tibaldi, L. C. Henriksen, M. H. Hansen, and C. Bak, "Wind turbine fatigue damage evaluation based on a linear model and a spectral method," *Wind Energy*, vol. 19, pp. 1289–1306, 2016.
[4] C. Pavese, C. Tibaldi, T. J. Larsen, T. Kim, and K. Thomsen, "Reduced Design Load Basis for Ultimate Blade Loads Estimation in Multidisciplinary Design Optimization Frameworks," *Journal of Physics: Conference Series*, vol. 753, no. 6, 2016.
[5] F. Zahle, C. Tibaldi, C. Pavese, M. K. McWilliam, J. P. A. A. Blasques, and M. H. Hansen, "Design of an Aeroelastically Tailored 10 MW Wind Turbine Rotor," *Journal of Physics: Conference Series*, vol. 753, 2016.
[6] C. L. Bottasso, F. Campagnolo, and A. Croce, "Multi-disciplinary constrained optimization of wind turbines," *Multibody System Dynamics*, vol. 27, no. 1, pp. 21–53, 2012.
[7] P. Bortolotti, C. L. Bottasso, and A. Croce, "Combined preliminary-detailed design of wind turbines," *Wind Energy Science*, vol. 1, no. 1, pp. 71–88, 2016.
[8] T. Macquart, V. Maes, D. Langston, A. Pirrera, and P. M. Weaver, "A New Optimisation Framework for Investigating Wind Turbine Blade Designs," in *12th World Congress of Structural and Multidisciplinary Optimization*, 2017.
[9] S. Scott, T. Macquart, C. Rodriguez, P. Greaves, P. McKeever, P. Weaver, and A. Pirrera, "Preliminary validation of ATOM: an aero-servo-elastic design tool for next generation wind turbines," *Journal of Physics: Conference Series*, 2019.
[10] International Electrotechnical Commission, *IEC 61400-1: Wind turbines - Part 1: Design requirements*. IEC, 3rd ed., 2005.
[11] DNV-GL, "DNVGL-ST-0376 Rotor blades for wind turbines," no. December, 2015.
[12] K. Svanberg, "MMA and GCMMA - two methods for nonlinear optimization, versions September 2007," *Technical report, Optimization and Systems Theory*, vol. 1, 2007.
[13] P. Chaviaropoulos, F. Rasmussen, A. B. Abrahamsen, D. Conti, A. Natarajan, G. Roukis, A. Makris, L. Sartori, F. Bellini, A. Croce, H. Polinder, D. Kaufer, J. A. Armendariz, A. Kumar, D. Powell, P. Todd, and R. Clark, "PI-based assessment (application) on the results of WP2-WP4 for 20 MW wind turbines," *INNWIND Deliverables*, 2017.
[14] L. Sartori, F. Bellini, A. Croce, and C. L. Bottasso, "Preliminary design and optimization of a 20MW reference wind turbine," *Journal of Physics: Conference Series*, vol. 1037, no. 4, 2018.
[15] T. Macquart, A. Pirrera, and P. Weaver, "A Finite Beam Element Framework for Variable Stiffness Structures," *25th AIAA/AHS Adaptive Structures Conference*, pp. 1–16, 2017.
[16] T. Macquart, S. Scott, P. Greaves, P. M. Weaver, and A. Pirrera, "Corotational Finite Element Formulation for Static Nonlinear Analyses with Enriched Beam Elements," *AIAA Journal*, pp. 1–17, 2020.
[17] C. L. Bottasso, F. Campagnolo, A. Croce, S. Dilli, F. Gualdoni, and M. B. Nielsen, "Structural optimization of wind turbine rotor blades by multilevel sectional/multibody/3D-FEM analysis," *Multibody System Dynamics*, vol. 32, no. 1, 2014.
[18] N. M. K. Poon and J. R. R. A. Martins, "An adaptive approach to constraint aggregation using adjoint sensitivity analysis," *Structural and Multidisciplinary Optimization*, vol. 34, 2007.
[19] J. H. Sjølund and E. Lund, "Structural gradient based sizing optimization of wind turbine blades with fixed outer geometry," *Composite Structures*, vol. 203, pp. 725–739, 2018.